sLHC Project Note 0007

2009-11-02

jim@stovall.net

RF Breakdown in Drift Tube Linacs

J. Stovall / BE-ABP, S. Ramberger / BE-RF, R. Lown / Aster Enterprises, Inc.

Summary

The highest RF electric field in drift-tube linacs (DTLs) often occurs on the face of the first drift tube. Typically this drift tube contains a quadrupole focusing magnet whose fringing fields penetrate the face of the drift tube parallel to the RF electric fields in the accelerating gap. It has been shown that the threshold for RF breakdown in RF cavities may be reduced in the presence of a static magnetic field. This note offers a "rule of thumb" for picking the maximum "safe" surface electric field in DTLs based on these measurements.

1.   Introduction

The highest RF electric field in drift-tube linacs (DTLs) often occurs on the face of the first drift tube. Typically this drift tube contains a quadrupole focusing magnet whose fringing fields penetrate the face of the drift tube parallel to the RF electric fields in the accelerating gap. A. Moretti et. al. have shown that the threshold for RF breakdown in RF cavities may be reduced in the presence of a static magnetic field (1). This note offers a "rule of thumb" for picking the maximum "safe" surface electric field in DTLs based on these measurements.

2.   RF breakdown in drift-tube linacs

Linac designers often want high accelerating fields in the initial gaps of DTLs to maximize energy gain and longitudinal acceptance. The risk, however, is that, if the resulting surface field is too high, RF breakdown can occur. Figure 1 shows the damage on the face of the initial drift tubes in the Los Alamos DTL resulting from RF breakdown. This damage was accompanied by a coating of "copper dust," comprised of copper microspheres, covering the bottom of the cavity indicating that the discharges had melted or even vaporized copper from the faces of the drift tubes. In this design, the drift tubes have flat faces so that, although the peak surface electric field occurs at the inner nose radius, the entire face of the drift tube sees a uniformly high field as well.

We believe that plasma effects, driven by the ionization of desorbed gases, are the dominant cause of RF breakdown. In addition we believe that the probability of breakdown is statistically proportional the surface area exposed to the maximum field. After a period of conditioning, even the Los Alamos DTL "cleaned-up" and is routinely operated without breakdown.

This is an internal CERN publication and does not necessarily reflect the views of the CERN management.

Figure 1. Initial drift tubes in the Los Alamos DTL showing arcing damage.

Breakdown thresholds were studied and quantified by W.D. Kilpatrick (2) in 1957 as a function of RF frequency. Figure 2 shows the empirically derived "Kilpatrick Criteria" (E_K) which is used by all linac designers in selecting the "bravery factor" for peak electric fields in RF cavities.

$$f = 1.64 \, E_K \, e^{-8.5/E_K}$$

f is the cavity frequency in MHz and E_K is the expected breakdown threshold in MV/m. As a result of improvements in cavity materials (OFE Copper in particular), cleanliness and vacuum technology, today it is not uncommon for some structures to operate at fields as high as 1.8 E_K over limited surface areas with negligible breakdown events.
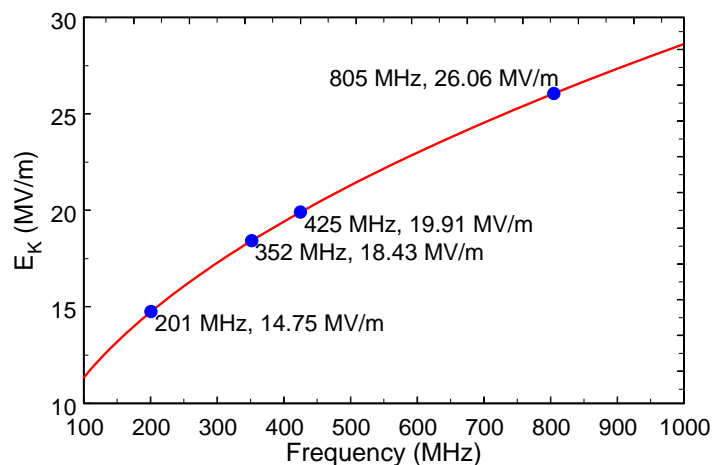

Figure 2. Kilpatrick criteria.

Figure 3 shows the electric field pattern in the first gap of the CERN Linac4 DTL reference design. In this drift-tube design there is a 11 mm "flat" that helps concentrate the accelerating field on axis and a 30° "face angle" that helps eliminate

multipactor. Figure 4 shows the corresponding surface electric field on the face of the drift tube (vertical axis) where we see that the highest value occurs on the inner nose radius, r_i. The corner radius, r_c, also enhances the surface field and is typically made as large as possible consistent with the other design constraints to minimize this effect. In this design, operating at 352 MHz, the peak surface field is 29.6 MV/m or 1.6 E_K at the design axial field E_0=3.1 MV/m.
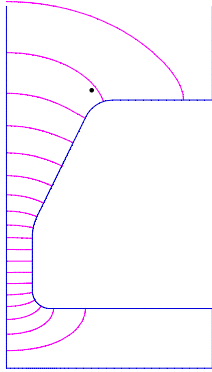

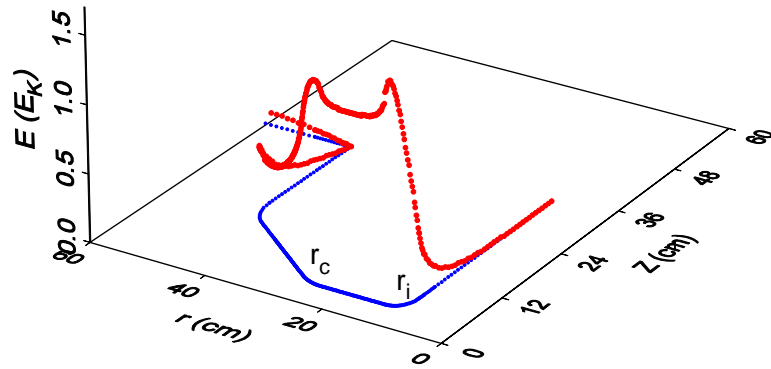Figure 3. Electric field pattern in the first gap of Linac4.

Figure 4. Surface electric field on the 1st drift tube of Linac4.

3.   Effect of magnetic fields on breakdown in RF cavities

We have long suspected that the presence of magnetic fringing fields from the quadrupole might enhance the sparking potential on low-energy drift tubes. In the case of the Los Alamos Linac, each drift tube contains an electromagnetic quadrupole lens that has large fringe fields due to flux leakage between the small number of water-cooled current windings on each pole.

In the 1970s we began using permanent magnet quadrupoles (PMQs) in DTLs to facilitate the use of higher frequency resonant structures and the design of more compact linacs. PMQs typically have very little flux leakage from the face of the pole pieces however there is still a fringing field originating from the pole tips that can penetrate the face of the drift tube near the nose. Figure 5 shows a low-energy drift tube from a Los Alamos DTL that operated at 425 MHz that contains a segmented PMQ. Figure 6 shows the magnetic field pattern in an x-y plane a few mm from the face of a typical PMQ comprised of rectangular blocks of SmCo, near where the face of the drift tube would be. One can clearly see the quadrupolar pattern of the PMQ fringing field reproduced in the discoloration of the RF surface of the drift tube indicating that it indeed plays some role in the RF surface conditioning. This drift tube had essentially flat faces so the pattern could be the result of either breakdown or persistent multipactor.

Multipactor between parallel surfaces is enhanced in the presence of magnetic lines that confine the electron trajectories. Angled faces cause the electron trajectories to "walk out" extinguishing the cascade.

There are two interesting features in figure 5 unrelated to the enhancement of breakdown. The quadrupolar pattern is visibly rotated about 2° from being square with the stem. This was later verified as a mechanical error in the design. Second we note that there is a light-colored line etched across the drift-tube face near the

aperture. This is the result of stripped H⁻ ions that are horizontally defocused by the previous lens. This mark occurred only on the upstream faces of the low energy drift tubes and alternate between horizontal and vertical.

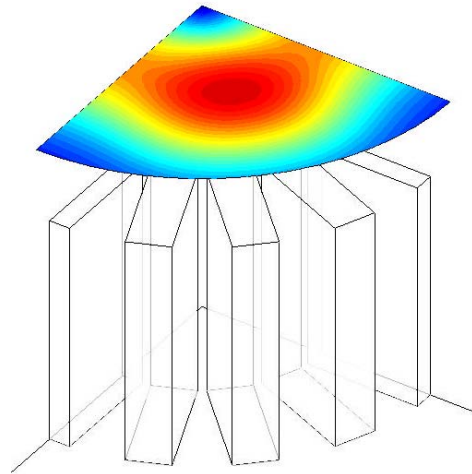Figure 5. 425 MHz drift tube showing the PMQ fringe-field pattern.

Figure 6. Typical PMQ fringing field near the drift tube face.

J. Norem (3) has demonstrated, in a pillbox test cavity operating at 805 MHz, that RF breakdown can occur when the local tensile stresses, exerted by electric fields, exceed the tensile strength of the parent material. He further proposes that the application of a collinear magnetic field can increase the mechanical forces by applying a torque to an emitter.

A. Morretti (1) and others have made extensive measurements of RF breakdown thresholds in this cavity in the presence of a dc magnetic field. The results of their measurements are reproduced in figure 7. The blue dots in this plot represent the measured breakdown threshold in an 805 MHz cavity observed at different values of dc magnetic field applied at the cavity's surface, expressed here in units of E_K. The curve represents a cubic fit to the data. We refer to this curve as the "Moretti criteria" and make the unsupported assumption that the effect scales with frequency over the range of interest (200-1000 MHz).
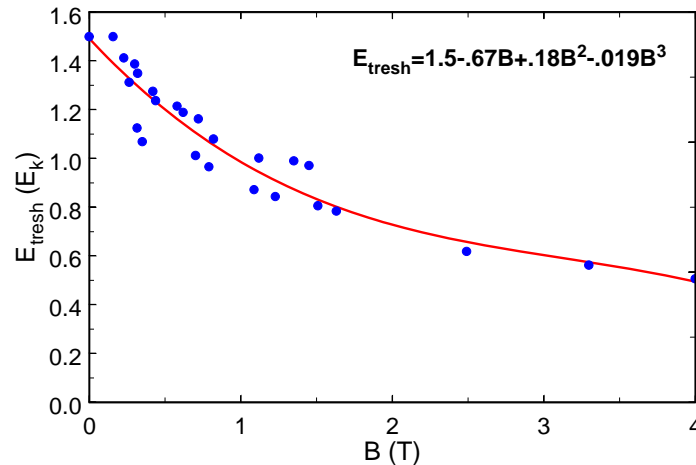

$$E_{tresh} = 1.5 - .67B + .18B^2 - .019B^3$$

Figure 7. Moretti criteria; breakdown threshold in the presence of a dc magnetic field.

4.   Enhanced breakdown threshold criteria applied to Linac4

Figure 8 is a picture of the prototype PMQ for the Linac4 tank 1 drift tubes. Figure 9 shows schematically how the PMQ is located in the initial drift tube and its field distribution B_y at a radius of 1 mm from the beam axis. We see that, because of the large aperture-to-length ratio, a significant amount of the integrated field lies in the fringe and extends into the accelerating gap. In fact we can see that the magnitude of the field has dropped to only ~50% of its central value at the edge of the PMQ and to ~12% of its central value at the nose of the first drift tube, the location of the highest surface RF electric field.
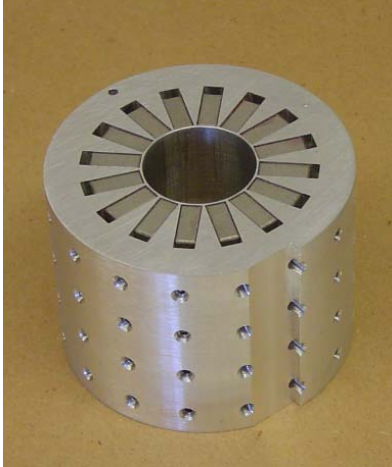

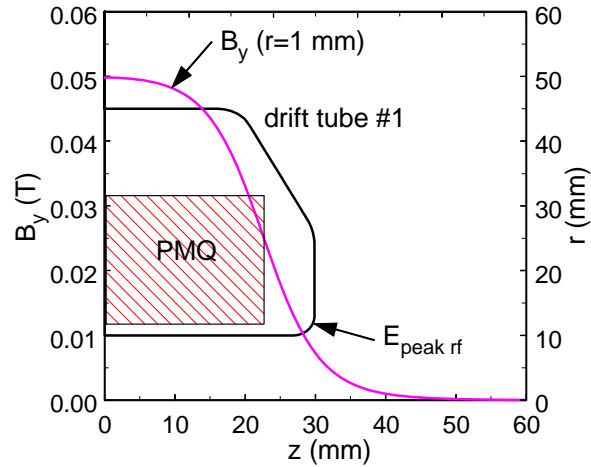Figure 8. Linac4 PMQ prototype.   Figure 9. Axial profile of B_y at a radius of 1 mm.

The field map of the PMQ shows that highest fields in the fringe occur in the r-z plane of the poles where there is no azimuthal component. Figure 10 shows the fringe field pattern in one quadrant of this PMQ in the r-z plane of a pole. We see that there is very little flux originating from the end face of the assembly and that most of the fringe field originates from the pole tip. Figure 11 shows the radial distribution of the fringe field at different distances from the PMQ. In this plot the axial dimension is measured from the centre of the PMQ which corresponds to the centre of the drift tube.
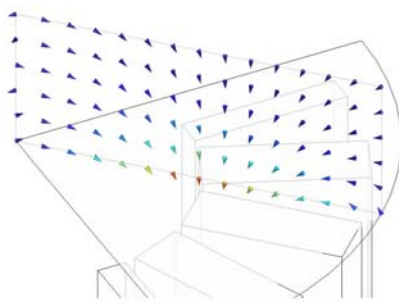

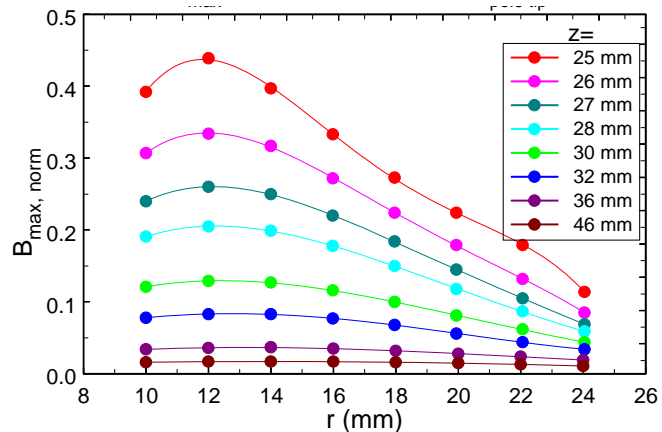Figure 10. Map of the PMQ fringe field in the r-z plane of one pole.

Figure 11. Maximum B field, normalized to the effective pole-tip B field, as a function of radius at different axial locations.

PMQs do not have poles in the traditional sense so their strength is typically characterized by their integrated gradient. We define an "effective pole-tip field" as the integrated gradient divided by the physical length of the assembly. This Linac4 PMQ has an integrated field of 2.29 T, a physical length of 45 mm and an effective pole-tip field of 0.508 T at a radius of 10 mm. The fringe fields in figure 11 are normalized to this effective pole-tip value.

Figure 11 shows that the highest B field in the fringe occurs at a radius of ~12 mm from the axis for all values of z. By coincidence this is the same radius at which the highest RF field E_{peak} occurs and at a point where the E and B fields are close to collinear.

Figure 12 shows the axial profile of the B field in the fringe of the PMQ normalized to the effective pole-tip value at a radius of 10 mm. By fitting a cubic to these values and assuming that the fields of every PMQ in tank 1 scale with the design gradient, we can evaluate the normalized fringe field for every PMQ using the following equation.

$$B_{max,norm,n} = 11.3 - 0.922z + 0.071910.02526z^2 - 0.000232z^3$$

$B_{max,norm,n}$ is the maximum value of the fringe field in the nth PMQ, that occurs in the plane of a pole 12 mm from the beam axis, normalized to the effective pole-tip field at 10 mm. z is the half length of the *nth* drift tube.
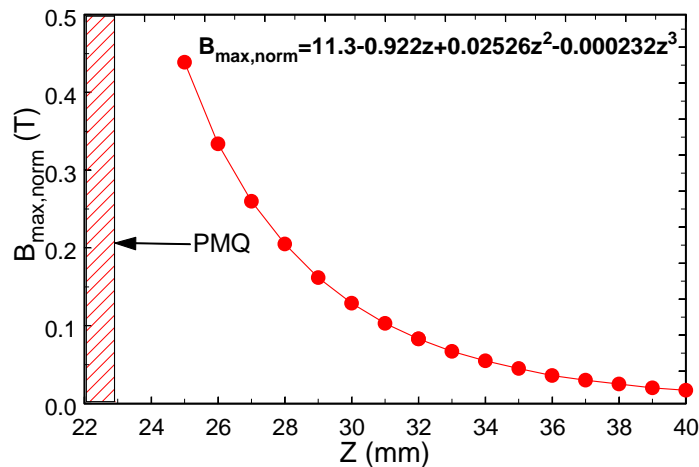

Figure 12. Axial distribution of the maximum B field in the PMQ fringe, normalized to the effective pole-tip field at 10 mm.

Using this equation we can calculate the magnetic field that penetrates the nose of the drift tubes in Linac4 as a function of the drift-tube length and design PMQ gradient. Figure 13 shows the expected maximum magnetic field on the nose of the first 14 drift tubes in tank 1 for two quadrupole laws FDFD & FFDD. From these B field values we can calculate the corresponding breakdown threshold E_{tresh} from the Moretti criteria which are shown in figure 14. Figure 14 also shows the design peak surface electric field on these drift tubes corresponding to the accelerating field of 3.1 MV/m. We can see in this figure that the design fields exceed the Moretti criteria by about 10%.

Because there is often very little flexibility in the design of the first drift tube the traditional way of reducing the surface field is to lower the design accelerating field,

E_0. This can be achieved by introducing a field ramp or keeping a flat but lower field throughout the tank. The Linac4 design will employ a different technique. Because the DTL follows a chopper line that contains three buncher cavities we want to keep its energy acceptance as large as possible. Partly because this DTL begins at 3 MeV, we have more flexibility in the design of the first drift tube. So to reduce the peak surface fields we will modify the shape of the initial drift tube faces by increasing the accelerating gap while preserving E_0 and adjusting the face angle to maintain resonance.
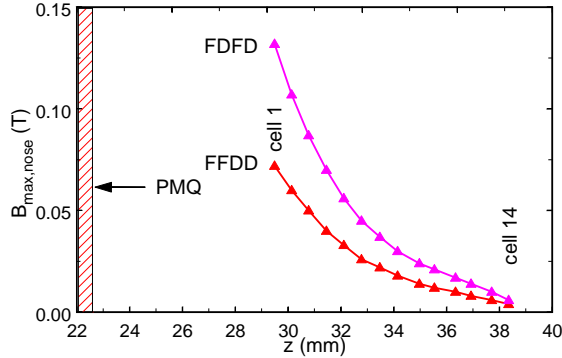

Figure 13. Magnetic field on the nose of the on the first 14 drift tubes.
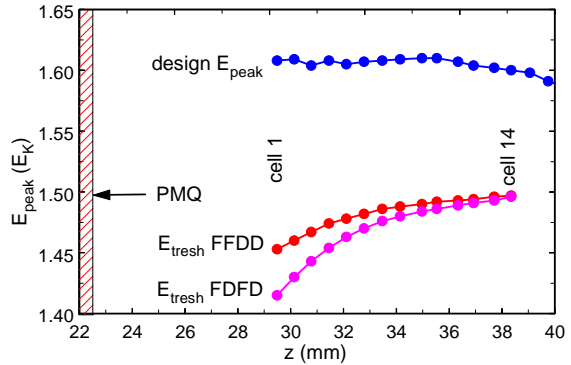
Figure 14. E_{tresh} , the sparking threshold on the first 14 drift tubes.

In the proposed example below, figure 15, we have also reduced the flat on the drift tubes from 11 to just 2 mm to reduce the potential of multipactor. Figure 16 shows the effect of increasing the gap. The field on the nose of the drift tube decreases linearly with increasing gap but, because the face of the drift tube comes into closer proximity to the PMQ, the sparking threshold also decreases. In cell 1 we find a solution where the curves cross at a gap of 10.5 mm, 1.5 mm longer than the initial design value. The face angle is reduced to 5.7° to maintain resonance. Figure 15 shows that there is still room to house the PMQ in the drift tube with this new geometry.
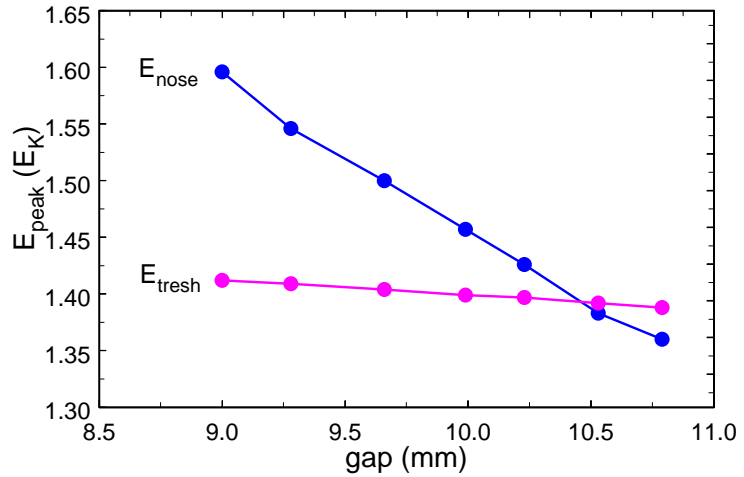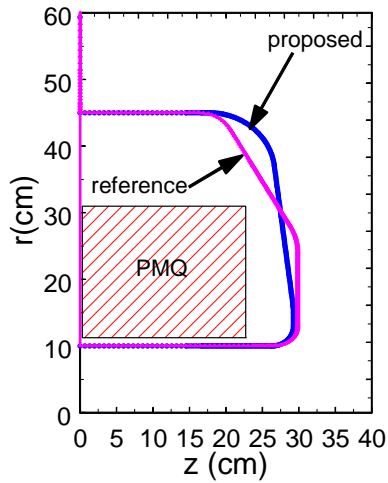
Figure 15. Proposed geometry for cell 1.   Figure 16. Peak surface electric field and sparking threshold in cell 1.

Figure 17 shows the electric field on the surface of both the reference face and the proposed shape modified to reduce the sparking threshold. Note that the field on the nose of the modified design, at r=12 mm, is reduced as is the field on the corner radius which initially also exceeded E_{tresh}. This modification reduces the transit time factor by ~1.5% and the shunt impedance by ~6%.
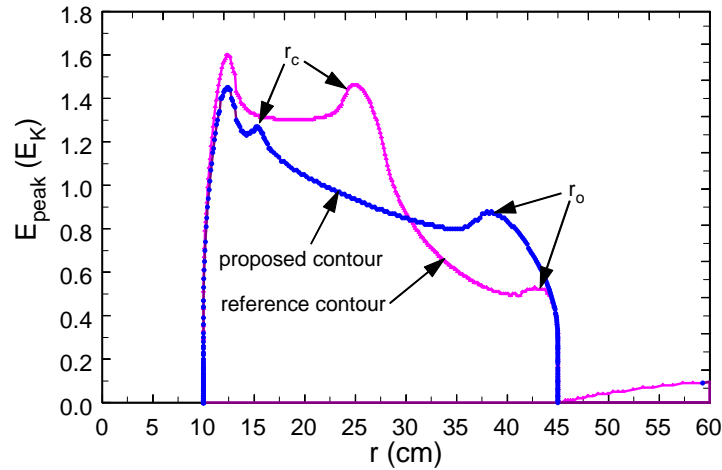
Figure 17. Surface field distribution on the reference and modified drift-tube designs.

5.   Field Clamps

An alternate approach to reducing sparking threshold on drift tubes is to reduce the magnetic field that penetrates the face of the drift tube. To achieve this we have tried adding a steel field clamp to each end of a PMQ. Figure 18 shows the magnetic field profile for such a magnet in which we have we have shortened the PMQ by 2 mm and added a 1 mm thick steel washer to each end. To provide the same focusing strength we have increased the effective pole-tip field so that the integrated field equals that of the unclamped magnet. Figure 18 shows the axial field profiles of both the clamped and unclamped PMQ measured at a radius of 10 mm from the axis.
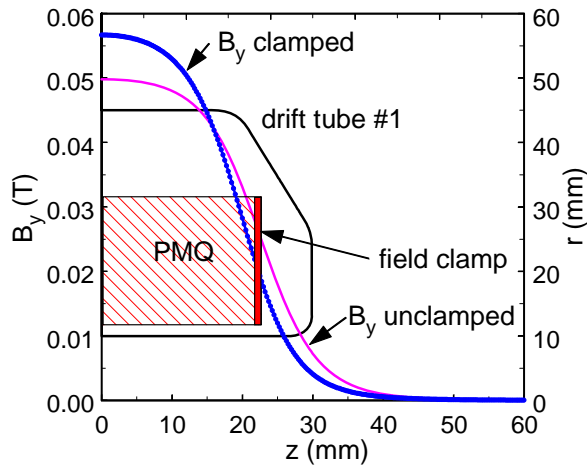
Figure 18. Magnetic field profile for clamped and unclamped PMQs having the same integral field.

The clamp does an effective job of reducing the fringe field however it also appears to "homogenize" it. We see in the field map that the maximum value of the field in the fringe no longer occurs in the r-z plane of a pole. Figure 19 shows the fringe field, normalized to the effective pole-tip field, in the x-y plane 2.5 mm from the field clamp where we see that it has lost its quadrupolar character and presumably its harmonic purity. If this is, in fact the case, it would be an unsuitable solution. Ignoring this complication for the moment, we see in figure 20 that the field clamp significantly reduces the axial field profile, measured at a radius of 12 mm (as compared with figure 12).
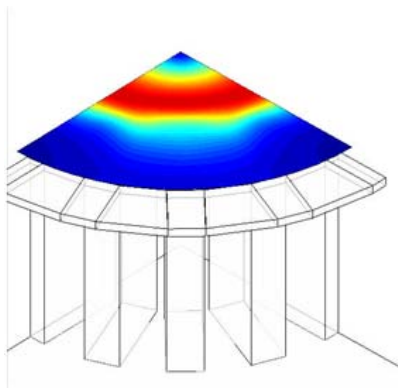

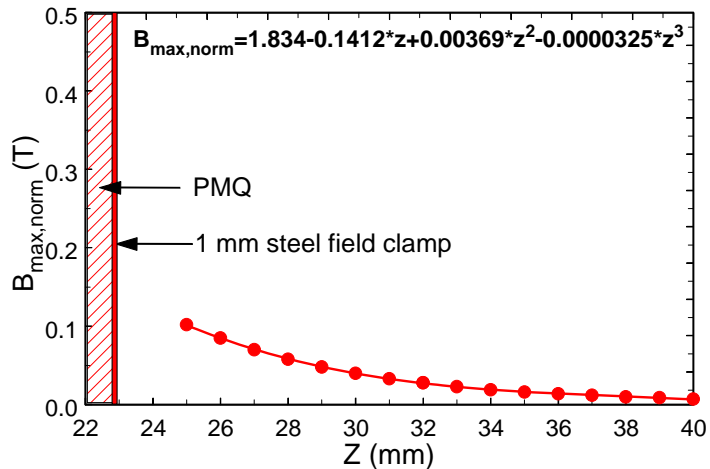Figure 19. B field 2.5 mm from the end of the PMQ having a 1-mm-thick steel field clamp.

Figure 20. Axial field profile of a clamped PMQ at r=12 mm.

Using a fit to this profile we can calculate the magnetic field that penetrates the nose of the drift tubes in Linac4 as a function of the drift-tube length and design gradient. Figure 22 shows the maximum magnetic field on the nose, B_{nose}, of the first 14 drift tubes in tank 1 using clamped PMQs following the FFDD quadrupole law. This figure also shows the corresponding sparking threshold, E_{tresh}, based on the Moretti criteria. Finally this figure shows the peak surface electric field, E_{peak}, on

these drift tubes corresponding to the design accelerating field. Using clamped PMQs we can see that the design fields still exceed the Moretti criteria by about 8.5%.
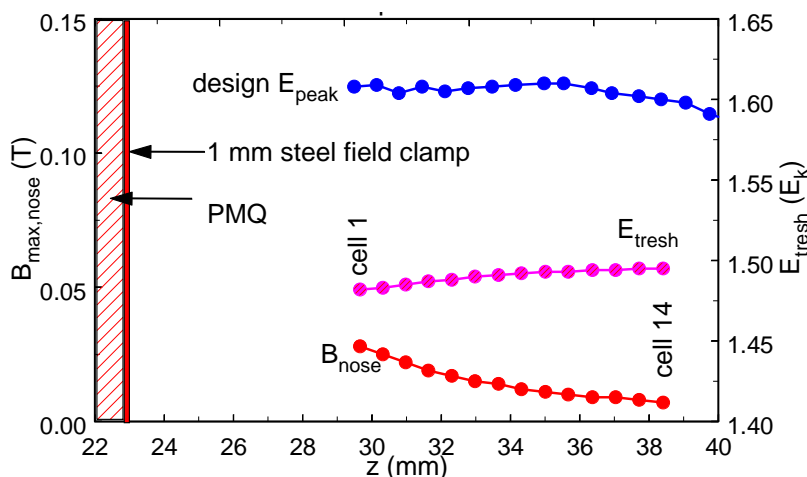

Figure 21. Moretti criteria applied to clamped PMQs in tank 1.

6.   Conclusions

The Moretti criteria can be a useful "rule-of-thumb" in designing DTLs to avoid RF breakdown. This criteria is based on empirical observations in an 805-MHz cavity to which we apply the unsupported assumption that the breakdown threshold scales with frequency. In applying this criterion we further make the unsupported assumption that the magnitude of the fringe field at the location of the drift tube nose scales with the effective pole tip field for PMQs of similar design.

While clamping the fields in PMQs can be an effective method for reducing the fringe fields it may also destroy the harmonic purity of the integrated field, making it unsuitable for DTLs. At best, reducing the fringe fields to zero can only increase the breakdown threshold to 1.5 E_K, according to the Moretti criteria. In other words, applying this rule of thumb would limit the surface fields in DTLs to this value.

Because of the scatter in the Moretti data, one can easily conceive of a weighted fit that intersects the vertical axis (B=0.0) at 1.6 E_K. The peak surface field in the initial cells of Linac4 is 1.6 E_K. The risk of breakdown results from approximately equal contributions of the RF E field and the PMQ fringe field. We are presently in the process of testing the Linac4 design geometry at full field both with and without PMQs. We expect the results of these measurements to give us a new calibration on the Moretti criteria at 352 MHz.

References

1. *Effects of high solenoidal magnetic fieslas on rf accelerator cavities.* **A. Moretti, Z. Qian, J. Norem, Y. Torun, D. Li & M. Zisman.** s.l. : Phys. Rev.ST Accel. Beams, 2005, Vol. 8.

2. *Criterion for Vacuum Sparking Designed to Include Both rf and dc.* **Kilpatrick, W.D.** 10, s.l. : RSI, 1957, Vol. 28.

3. *Dark current breakdown, and magnetic field effects in a multicell, 805 MHz cavity.* **J. Norem, V.Wu, A. Moretti, M.Popovic, Z.Qian, Y.Torun & N. Solome.** s.l. : Phys. Rev. ST Accel. Beams, 2003, Vol. 6.